Biomaterials Science

Engineering blood-brain barrier microphysiological systems to model Alzheimer's disease monocyte penetration and infiltration

Journal:	*Biomaterials Science*
Manuscript ID	BM-ART-02-2025-000204.R1
Article Type:	Paper
Date Submitted by the Author:	22-Apr-2025

Complete List of Authors:	Gu, Longju; Indiana University Bloomington Mao, Xiangdi; Indiana University Bloomington Tian, Chunhui; Indiana University Bloomington Yang, Yang; Indiana University Bloomington Yang, Kaiyuan; Indiana University Bloomington Canfield, Scott; Indiana University School of Medicine Zhu, Donghui; Stony Brook University, Biomedical Engineering Gu, Mingxia; UCLA Guo, Feng; Indiana University Bloomington, Intelligent Systems Engineering

Engineering blood-brain barrier microphysiological systems to model Alzheimer's disease monocyte penetration and infiltration

Longjun Gu,[1] Xiangdi Mao,[1] Chunhui Tian,[1] Yang Yang,[1] Kaiyuan Yang,[1] Scott G. Canfield,[2,3] Donghui Zhu,[4] Mingxia Gu,[5] and Feng Guo[1]

1. Department of Intelligent Systems Engineering, Indiana University, Bloomington, IN 47405, United States
2. Stark Neurosciences Research Institute, Indiana University School of Medicine, Indianapolis, IN, 46202, United States
3. Department of Anatomy, Cell Biology, and Physiology, Indiana University School of Medicine, Terre Haute, IN, 47809, United States
4. Department of Biomedical Engineering, University of Stony Brook, 100 Nicolls Rd, Stony Brook, NY, 11794, United States
5. Department of Anesthesiology and Perioperative Medicine, David Geffen School of Medicine, Eli and Edythe Broad Center for Regenerative Medicine and Stem Cell Biology, University of California, Los Angeles, CA 90095, United States

Corresponding email address: fengguo@iu.edu (F.G.).

Abstract

Alzheimer's disease (AD) is a progressive and neurodegenerative disease, predominantly causing dementia. Despite increasing clinical evidence suggesting the involvement of peripheral immune cells such as monocytes in AD pathology, dynamic penetration and infiltration of monocytes crossing blood-brain barrier (BBB) and inducing neuroinflammation is largely understudied in an AD brain. Herein, we engineer BBB-like microphysiological systems (BBB-MPS) models for recapitulating the dynamic penetration and infiltration of monocytes in an AD patient's brain. Each BBB-MPS model can be engineered by integrating a functional BBB-like structure on a human cortical organoid using a 3D-printed device within a well of a plate. By coculturing these BBB-MPS models with monocytes from AD patients and age-matched health donors, we found that AD monocytes exhibit significantly greater BBB penetration and brain infiltration compared to age-matched control monocytes. Moreover, we also tested the interventions including Minocycline and Bindarit, and found they can effectively inhibit AD monocyte infiltration, subsequently reducing neuroinflammation and neuronal apoptosis. We believe these scalable and user-friendly BBB-MPS models may hold promising potential in modeling and advancing therapeutics for neurodegenerative and neuroinflammatory diseases.

Key words

Brain organoid, Blood-brain barrier, Microphysiological system, Monocyte penetration, Neuroimmune interaction

Introduction

Alzheimer's disease (AD) is a progressive neurodegenerative disorder that primarily impairs memory, thinking, social skills, and behavior[1, 2]. It is the most common cause of dementia among older adults and is quickly becoming one of the most expensive, lethal, and burdening diseases of this century[3, 4]. Although current therapeutic strategies for AD effectively aim to improve symptoms or slow disease progression, a definitive cure has yet to be discovered. One premising perspective is to innovate therapeutics targeting the neuroinflammation in AD. The immune system plays a vital role in the development and progression of AD[5, 6]. Research on brain-resident immune cells in the progression of AD is extensive, yet studies on the peripheral immune system remain limited[7-10]. As one of the most important peripheral innate immune cells in the blood, monocytes can be recruited into the CNS due to the increasing permeability of blood-brain barrier (BBB) in AD and participate in AD development[11-14]. Specifically, the CC-chemokine ligand 2 (CCL2) generated by activated microglia and astrocytes binds to the C-C motif chemokine receptor (CCR2) on monocytes and mediates the recruitment of these monocytes. Once recruited, monocytes are directed to the BBB, where they undergo diapedesis, a process that enables them to penetrate through the BBB and infiltrate into the brain parenchyma[15-19]. The activation of infiltrated monocytes also exacerbates neuroinflammation, leading to further neuronal damage and contributing to the progression of AD[20-22]. However, to date, the dynamics of monocytes penetrating BBB and infiltrating the brain parenchyma remain poorly understood in AD, partly due to the absence of suitable human models with functional BBB structures.

Current knowledge of monocytes' participation in AD progression primarily derives from animal models, particularly transgenic mouse models[23-25]. However, transgenic mouse models cannot adequately mimic the complex pathological features of AD[26]. On the one hand, transgenic mice models mainly simulate symptoms of familial AD, which accounts for only 2-5% of AD cases. On the other hand, there are significant neurophysiological differences between human and mouse brains across multiple bio-hierarchical levels, such as the morphogenesis and cytoarchitecture of the cortex, BBB tight junction and efflux expression and efflux transporter[27, 28] as well as the neuron polarization of neuroepithelium. Superior to animal models, emerging human brain organoid (hBO) provides a more human-relevant model to investigate neurological diseases[29, 30]. Human brain organoids derived from human pluripotent stem cells (hPSCs) can recapitulate some critical physiological features of the human brain, including cellular diversity, cytoarchitecture, and neural activities[31-34]. More importantly, hBOs can be derived from patient-specific induced PSCs, thereby accurately recapitulating the individual's unique genetic background and associated mutations[35, 36]. However, brain organoids encounter several significant challenges, including the absence of BBB structures and immune cells, as well as the limitation of oxygen and nutrient perfusion.

So far, efforts have been made to advance hBOs for neurological studies and disease modeling. By lowering the concentrations of the neuroectodermal stimulant heparin and delaying Matrigel embedding in the cerebral organoids, microglia naturally developed within these organoids, exhibiting characteristic ramified morphology and the capacity to mediate inflammatory responses[29]. In addition, we have previously presented a tubular organoid-on-a-chip device by employing a three-dimensional (3D) printed hollow mesh scaffold to improve oxygen and nutrient perfusion and further reduce the hypoxia and necrosis of organoids[30]. Microglia incorporated into the device were then exposed to an opioid receptor agonist to stimulate microglia-mediated neuroinflammation. Despite progress in investigating neuroimmune interactions with existing models, a major limitation persists in the absence of a model that can monitor the dynamic process by which peripheral innate immune cells, such as monocytes, cross the BBB and infiltrate

brain tissue. The lack of capability to observe these dynamics hinders a deeper understanding of how monocytes contribute to neuroinflammation and disease progression.

Herein, we engineered novel BBB-MPS models that incorporate human cortical organoids with an integrated BBB for recapitulating dynamic penetration and infiltration of monocytes in an AD brain. Our BBB-MPS models have several advantages: (1) The functional BBB-like structures are easily created by culturing endothelial cells and human brain organoids containing astrocytes on 3D-printed devices. (2) Our previously reported 3D-printed devices incorporate in situ air-liquid interface culture, promoting efficient nutrient and oxygen exchange. (3) Our devices are designed to be compatible with commercially available 24-well microtiter plates, allowing for the simultaneous investigation of multiple experimental conditions which include drug screening to inhibit the penetration of AD patient-derived monocytes and subsequently mitigate neuroinflammation. Applying novel BBB-MPS models, we monitor the dynamic infiltration of monocytes cross through BBB and demonstrate that reducing the penetration of AD monocytes through the BBB can effectively decrease neuroinflammation and neuronal apoptosis. Consequently, the BBB-MPS models hold significant potential for investigating the role of peripheral innate immune cells in neurodegenerative diseases.

Materials and methods

Design and fabrication of 3D-printed holder devices. Following the protocol that we developed previously[37-39], the holder devices were designed using AutoCAD software (Autodesk) and fabricated using a stereolithography 3D printer (Form 3B, Formlabs) and FormLabs Clear Resin V4. Design details of the holder device are shown in **Fig. S1**. The polyester porous membranes (Sterlitech) were cut by employing a CO_2 laser engraver and bonded to holder devices using double-sided adhesive (3M).

Human stem cell culture. The human embryonic stem cell (hESC) line (WA09) was purchased from WiCell institute. The cells were handled under the guidelines of both WiCell Institute and Indiana University Biosafety Committee. WA09 cells were cultured with mTESR plus medium (Stemcell Technologies) on Growth Factor Reduced Matrigel (Corning) coated 6-well plates in a humidified incubator at 37ºC and 5% CO_2. The medium was changed every other day. WA09 cells were passed every 5 days using ReLeSR (Stemcell Technologies).

Generation of human cortical organoids. Human cortical organoids were fabricated from the hESC line (WA09). The cortical organoids were cultured according to a previously reported protocol[40, 41]. The detailed composition of cortical organoid differentiation medium is described in Table S1. Specifically, embryonic bodies (EBs) were generated using a 96-well U bottom microplate (Sarstedt) by aggregation of ~9,000 hESCs per well and then cultured in 100 µL cortical organoid medium 1 (COM I). After EB formation (Day 1), the EBs were switched to COM I without Y-27632. After 3 days of culture, the cultures were transferred to cortical organoid medium 2 (COM II) for the next 7 days. On day 10, the cultures were maintained in cortical organoid medium 3 (COM III) for 7 days, followed by 7 additional days in cortical organoid medium 4 (COM IV). Next, the cultures were transferred to cortical organoid medium 5 (COM V) to facilitate maturation, glycogenesis, and enhance cellular activity. After 22 days, the cortical organoids were maintained in cortical organoid medium 6 (COM VI). Medium change was performed every other day during this process except when specified. From day 30 on, the organoid cultures were transferred to a 6-well ultralow adhesion plate (Corning) and kept on an orbital shaker at the speed of 90 rpm. The immunofluorescence characterization of the cortical organoids is shown in **Fig. S2**.

Human umbilical vein endothelial cell culture. Human umbilical vein endothelial cells (HUVECs) were cultured in endothelial cell growth medium (Lonza) in 6-well microtiter plates. After confluence, HUVECs were digested with 0.25% trypsin ethylenediaminetetraacetic acid (EDTA) (Gibco) and used for the following experiments. To minimize experimental variability, only the primary cells in passages 6-8 were used for experiments.

Permeability assay. The permeability of the BBB-MPS was tested by using 70 kDa dextran (Invitrogen) using our well-developed protocol[42]. Briefly, the BBB-MPS was culture in 1 mL culture medium. The 50 μL of 500 μg/mL dextran were prepared in the culture medium and replaced the medium in the holder devices from the BBB side. The holder devices were placed in an incubator for 30 min. Then, the medium in the bottom well was collected and the fluorescence was quantified at 555/580 nm (excitation/emission, Gain: 65) using a microplate reader. A standard curve was made of 500 μg/mL dextran, and the apparent permeability coefficient (P_{app}) was calculated according to the equation below:

$$P_{app}(cm/s) = \frac{V_t \times C_t}{A \times C_0 \times t}$$

where V_t is the measured volume of the bottom well, C_t is the measured dextran concentration at time t, A is the effective permeability area of the membrane, and C_0 is the original dextran concentration.

Isolation of monocytes from human PBMCs. Peripheral blood mononuclear cells (PBMCs) were isolated from blood samples obtained from different healthy donors and AD patients. Monocytes were isolated from PBMCs using the Classical Monocyte Isolation Kit according to the manufacturer's protocol (Miltenyi Biotec GmbH) with MS Column (Miltenyi Biotec GmbH). Typically, 5×10^4 monocytes per milliliter of whole blood were obtained. All experiments were performed in accordance with the guidelines of Indiana University biological sample procurement and biobanking protocol, and experiments were approved by the ethics committee at Indiana university. Informed consents were obtained from human participants of this study.

Imagining monocyte infiltration. Monocyte infiltration was characterized by adapting our developed protocols previously[43-46]. The monocytes were labeled with Vybrant DiL (red) (Invitrogen) at 1:1000 dilutions at 37°C for 30 min before being introduced into BBB-MPS models. Simultaneously, the BBB-MPS models were labeled with Vybrant DiO (green) (Invitrogen) at 1:1000 dilutions at 37°C for 30 min. A total of 1×10^5 labeled monocytes were added to each BBB-MPS. After co-culturing in a 37°C incubator for 24 h, the BBB-MPS models were imaged using an Olympus OSR spinning disk confocal microscopy with a 10× objective inside a Tokai Hit on-stage incubator set at 37°C and 5% CO_2. The acquired Z-stack images were analyzed using Imaris (version 9.0.1). A 3D reconstruction of the BBB-MPS structure was generated based on the DiO signal to define the boundary of the organoid. Monocytes (DiI signal) were detected and segmented using the software's spot detection function. Only monocytes located within the reconstructed 3D boundary were considered infiltrated. The infiltrated rate was defined as the percentage of infiltrated monocytes out of the total number of monocytes added to the system.

Drug treatment. Minocycline (STEMCELL Technologies) 20 to or 100 μM Bindarit (Cayman Chemical) were used for BBB-MPS model treatment with the addition of 1×10^5 labeled monocytes. The co-culture was then incubated at 37°C for 24 h before confocal imaging.

Cryo-sectioning of BBB-MPS. Cryo-sectioning of the BBB-MPS was conducted using our well-developed protocol[47]. Samples were initially rinsed twice with 1× PBS and fixed in 4% paraformaldehyde (Thermo Fisher) in 1× PBS at 4°C overnight. Post-fixation, samples were cryoprotected by immersion in 30% sucrose (Sigma) in 1× PBS (w/v) at 4°C overnight. The

cryoprotected samples were then embedded in the O.C.T. compound (Fisher Scientific) using cryomolds (Sakura Finetek USA) and frozen on dry ice. After that, the frozen samples were sectioned to a thickness of 30 μm using a cryostat (Epredia) and collected on Superfrost™ Plus microscope slides (VWR).

Immunofluorescence staining. Immunofluorescence staining was conducted directly on cryosectioned samples collected on slides. The sections were washed twice with 1× PBS to remove residual O.C.T. compound. Antigen retrieval was performed by treating the sections with sodium citrate buffer (Sigma) for 20 minutes. After rinsing twice with 1× PBS, the sections were permeabilized and blocked using 0.3% Triton X-100/5% normal donkey serum (Jackson ImmunoResearch) in 1× PBS for 1 hour. Primary antibodies were then applied in a diluted antibody solution and incubated overnight at 4°C, humidified chamber. The slides were subsequently rinsed three times with 1× PBS and incubated with secondary antibodies at room temperature for 2 hours. Finally, the sections were washed three times with 1× PBS, and coverslips were mounted using ProLong Gold Antifade Mountant with DAPI (Invitrogen). Detailed antibody information and dilution factors are shown in **Table S2**.

Quantification of astrocyte activation and neuronal apoptosis. Astrocyte activation quantification was conducted based on immunofluorescence slides stained with an anti-GFAP antibody. Neuronal apoptosis was quantified with immunofluorescence slides stained with anti-NeuN and anti-cleaved caspase-3 antibodies. One staining slide per cortical organoid was selected for quantification. The visualization was conducted using a laser scanning confocal microscopy (Stellaris 8, Leica). The quantification of fluorescence intensity and cell ratio was performed with ImageJ (v 1.54f). The value obtained from one slide per organoid was presented as one data point in the results.

Statistical analysis. The statistical comparison of each group was performed via t-test with GraphPad Prism 8 (GraphPad Software). All data are presented as mean ± SEM values. The statistical significance of differences in values is denoted as following *: $p < 0.05$, **: $p < 0.01$, ***: $p < 0.005$.

Results

Engineering BBB-MPS models to study dynamic penetration and infiltration of AD monocytes. In AD, monocytes migrate from the bloodstream into the brain by penetrating the BBB, resulting in infiltration in the brain parenchyma[48, 49]. Within the AD brain, these infiltrating monocytes become activated in response to Aβ plaques and other pathological stimuli, releasing pro-inflammatory cytokines such as necrosis factor-alpha (TNF-α), interleukin-1 beta (IL-1β), and interleukin-6 (IL-6). This inflammatory cascade exacerbates neuronal damage, amplifies neuroinflammation, and contributes to the neurodegenerative processes that are hallmark features of AD pathology (**Fig. 1a**)[10, 20, 48]. We engineered BBB-MPS models to precisely observe the penetration and infiltration process of the monocytes from BBB to the cortical brain (**Fig. 1b** and **Fig. S3**). In the microphysiological system, the human umbilical vein endothelial cell (HUVEC) monolayer (upside) and cortical organoids (downside) were located on both sides of the polyester porous membrane of the 3D-printed holder device. Based on the previous instruction, cortical organoids were cultured on the air-liquid interface to improve oxygen and nutrient exchanges and to mediate the formation of organoids with flattened shapes[50-53]. It is well mentioned that the BBB-MPS models are compatible with the current commercial microtiter plates and thus are applied for high-throughput and user-friendly drug screening aiming at mitigating neuroinflammation induced by AD patient-derived monocytes. Furthermore, the robustness and simplicity of the model allow users to easily “switch-out” cell types to incorporate various BBB-like cell types and disease-specific organoids. Immunofluorescent staining showed that after co-culture with BBB-

MPS models for 48 h, $CD68^+$ monocytes derived from AD patients migrated through the endothelial monolayer into healthy cortical organoids (**Fig.1c**). Using the BBB-MPS model, we can dynamically monitor and assess monocyte penetration across the BBB and subsequent infiltration into the brain parenchyma.

Characterization of BBB-MPS models. The brain is regarded as an immune-privileged organ due to the protective role of the BBB. In BBB, endothelial cells are tightly aligned to form a continuous monolayer, while astrocytes enwrap the outer surface of these endothelial cells with their end-feet, enhancing the selective permeability and structural integrity of the barrier[45-49]. In AD, the BBB becomes increasingly susceptible to immune cell infiltration. This vulnerability arises from the upregulation of adhesion molecules, the breakdown of BBB tight junctions, and other processes exacerbated by both aging and disease pathology[50-53]. In the BBB-MPS models, HUVECs (upside) formed an integrated monolayer that positively expressed platelet endothelial cell adhesion molecule-1 (PECAM-1) as an endothelial cell marker, along with well-developed tight junction protein zonula occludens-1 (ZO-1) and adherent junction protein vascular endothelial cadherin (VE-cadherin) (**Fig. 2a**). On the cortical organoid side, astrocytes and mature neurons were identified by staining for glial fibrillary acidic protein (GFAP) and microtubule-associated protein 2 (MAP2), respectively (**Fig. 2b, Fig. S4**). The astrocytes in the BBB-MPS models extended their end-feet to wrap around endothelium (**Fig. 2c,d**). The paracellular permeability assay, a standard assessment of epithelial and endothelial barrier integrity, demonstrated that the permeability of the tracer marker, 70 kDa dextran, was lower in the BBB-MPS models, indicating that this microphysiological system possesses an integrated BBB (**Fig. 2e**). Taken together, the BBB-MPS effectively recapitulates the essential features of the BBB.

Investigation of monocyte infiltration using BBB-MPS models. As mentioned previously, monocytes exhibit an enhanced capacity to penetrate the BBB and infiltrate the brain parenchyma. To investigate the differential infiltration capacity of monocytes derived from AD patients compared to age-matched control individuals, we introduced primary monocytes isolated from PBMCs into BBB-MPS models. We collected the AD monocytes (AD/Mo) from the PBMCs of patients aged over 70 years and obtained age-matched control monocytes (AM/Mo) from donors of the same age group. After adding AD/Mo or AM/Mo to BBB-MPS models, they gradually penetrated the BBB and infiltrated the cortical organoids (**Fig. S5**). To quantify the infiltration of monocytes into cortical organoids, we analyzed the recorded images (**Fig. 3a**). We found that the infiltrated rate of AD/Mo was approximately twice that of age-matched AM/Mo (left in **Fig. 3b**). Furthermore, AD/Mo exhibited a greater infiltration depth (right in **Fig. 3b**), indicating that they possess a higher infiltration capacity than AM/Mo.

Minocycline and Bindarit treatments reduce neuroinflammation and neuronal apoptosis. Next, we investigate the effects of two promising therapeutic agents, Minocycline and Bindarit, on inhibiting the infiltration of monocytes into cortical organoids. Both Minocycline and Bindarit have anti-inflammatory and neuroprotective properties[54-57]. Notably, both Minocycline (50 μM) and Bindarit (25 μM) significantly suppressed the infiltrated rate and depth of monocytes derived from AD patients, indicating that these agents reduce monocyte infiltration in AD (**Fig. 3c, d** and **Fig. S6**). Additionally, it has been reported that infiltrating monocytes can amplify inflammatory responses in microglia and astrocytes within the CNS and further exacerbate neuronal damage[58-60]. We next explored the regulatory mechanism of Minocycline and Bindarit. GFAP staining was used to assess astrocyte activation, revealing that GFAP levels were significantly suppressed in both the Minocycline and Bindarit treatment groups compared to the AD/Mo group (**Fig. 4a, b**). We also evaluated the neuroprotective effects of Minocycline and Bindarit on neuronal apoptosis, potentially associated with neuroinflammation induced by AD monocytes. Neuron nucleus were labeled with NeuN, while apoptotic cells were labeled with cleaved caspase-3. Co-staining for

NeuN and cleaved caspase-3 indicated neuronal apoptosis in the AD/Mo group. The percentage of cleaved caspase-3-positive neurons in brain organoids was significantly reduced in the Minocycline and Bindarit treatment groups, suggesting that these two drugs might reverse AD monocyte-induced neuronal apoptosis by inhibiting monocytes penetration through BBB (**Fig. 4c-d**).

Discussion and conclusion

In this study, we engineered novel BBB-MPS models to investigate monocyte crossing BBB and the related neuroimmune interactions in AD. Our findings indicate that monocytes from AD patients have a significantly higher capacity to penetrate the BBB and infiltrate brain tissue than those from age-matched control individuals, underscoring their potential role in exacerbating neuroinflammation in AD. Furthermore, the therapeutic agents Minocycline and Bindarit markedly reduced monocyte infiltration, subsequently decreasing neuroinflammation and neuronal apoptosis. The BBB-MPS models thus provide a valuable platform for examining immune cell dynamics in neurodegenerative diseases and evaluating novel therapeutic approaches.

Dysregulation of the immune system is a key feature in AD, with immune cells undergoing dynamic changes throughout disease progression and fulfilling diverse roles. Monocytes, a type of white blood cell produced in bone marrow, are critical participants in AD pathology. Studies in amyloid precursor protein/presenilin 1 (APP/PS1) mouse models have shown that amyloid deposits in blood vessel walls interact with monocytes, which aid in clearing these deposits[61]. Once monocytes infiltrate the CNS via the CCL2/CCR2 axis[62-64], they modulate neuroinflammation and protect neuron synapses from the neurotoxic effects of Aβ42 oligomers[65]. Additionally, monocytes can transport Aβ to the bloodstream, reducing its accumulation in the brain[66]. However, these models predominantly capture monocyte activity through endpoint analyses, such as post-mortem tissue sampling, which only provides static representations of monocyte presence[67]. Consequently, the lack of dynamic observation limits our understanding of monocyte migration and interactions within the CNS, highlighting the need for human-based models capable of real-time observation. Our BBB-MPS models allow the real-time observation of monocyte penetration through the BBB and infiltration into brain organoids. The system consists of a 3D-printed holder device with a polyester porous membrane, compatible with standard 24-well microtiter plates and suitable for imaging techniques like fluorescence and confocal microscopy. HUVECs form a monolayer on one side of the membrane, mimicking the BBB, while cortical organoids are cultured on the opposite side to represent brain tissue. AD and age-matched monocytes are introduced on the BBB side, where they migrate towards the cortical organoids, enabling dynamic observation of this process. Our results demonstrate that AD-derived monocytes infiltrate brain tissue more effectively than those from healthy controls, emphasizing their role in AD pathology. This increased infiltration can be attributed to the factors, including the enhanced migratory capacity of AD monocytes, driven by elevated expression of receptors such as CCR1 and migration-related genes (e.g., SEMA6B, FGR, and FOXO3), which facilitate their penetrate through the BBB[68].

Blocking the infiltration of peripheral immune cells into the CNS presents a promising strategy for treating AD and other neurodegenerative disorders[69]. In this study, we explored the effects of two therapeutic agents, Minocycline and Bindarit, on reducing monocyte migration into the CNS. Minocycline has been demonstrated potentially as an AD therapeutic due to its anti-inflammatory and neuroprotective properties, including its ability to suppress the production of pro-inflammatory chemokines such as CCL2[54, 70]. Moreover, Minocycline can downregulate the expression of adhesion molecules on endothelial cells, which may help to limit monocyte infiltration into brain tissue. Bindarit, an anti-inflammatory small molecule, inhibits the synthesis of monocyte

chemoattractant proteins (MCPs) by modulating the NF-κB pathway[55, 56]. By targeting these chemokines, Bindarit reduces monocyte recruitment to sites of inflammation, thereby helping to regulate the inflammatory response. Our findings indicate that treatment with Minocycline and Bindarit significantly reduced both the number and depth of monocyte infiltration in cortical organoids. Furthermore, these agents alleviated AD-related neuropathology induced by monocyte infiltration, including astrocyte activation and neuronal apoptosis. These findings position the engineered BBB-MPS as a promising model for testing therapies aimed at regulating immune cell infiltration in AD and other neurodegenerative diseases.

While the current BBB-MPS model effectively simulates the BBB, it has some limitations. One limitation of current BBB-MPS models is that HUVECs cannot fully replicate the unique properties of brain endothelial cells such as specialized tight junctions and transport mechanisms. Moreover, the absence of pericytes limits the physiological relevance of the model, as pericytes are known to regulate BBB stability and immune cell trafficking[68]. Pericytes have been shown to secrete chemokines that facilitate monocyte recruitment and transmigration. Their interaction with infiltrating monocytes plays a key role in modulating neuroinflammation and BBB integrity under disease conditions[71, 72]. Furthermore, the current model lacks fluidic stimulation, which is crucial for mimicking blood flow and shear stress in vivo. Fluid shear stress plays a significant role in endothelial cell function, including the regulation of tight junctions and monocyte adhesion. To address these limitations, further development of the model could incorporate brain endothelial cells, pericytes, and fluidic stimulation to better replicate the in vivo conditions of the BBB[73, 74]. Additionally, our study focused on dynamically monitoring and evaluating the penetration of monocytes across the BBB and their subsequent infiltration into the brain parenchyma. While in AD, the BBB becomes compromised, leading to increased permeability and dysfunction. This disruption allows the entry of potentially harmful substances and immune cells into the brain. Conversely, the infiltrated immune cells further exacerbate BBB breakdown by releasing inflammatory mediators such as IL-1β and TNF-α, which impair endothelial integrity, exacerbate neuroinflammation, and contribute to neuronal damage[75, 76]. Further study can investigate how monocytes interact with and contribute to BBB breakdown in the context of AD. To obtain more disease-relevant insights, it will be critical to utilize models that incorporate patient-specific pathological features of AD, as the current models lack disease specificity and may not fully capture the complexity of the AD-associated BBB. To conclude, our BBB-MPS devices are simple, user-friendly, and compatible with microtiter plates and lab settings. We believe that the BBB-MPS holds considerable promise for exploring the involvement of peripheral innate immune cells in neurodegenerative diseases.

CRediT authorship contribution statement

Longjun Gu: Data curation, Investigation, Methodology, Validation, Visualization, Writing - original draft, Writing - review & editing. **Xiangdi Mao:** Data curation, Writing - review & editing. **Chunhui Tian:** Methodology, Writing - review & editing. **Yang Yang**: Data curation, Writing - review & editing. **Kaiyuan Yang:** Visualization, Writing - review & editing. **Scott G. Canfield:** Data curation, Writing - review & editing. **Donghui Zhu:** Data curation, Writing - review & editing. **Mingxia Gu:** Data curation, Writing - review & editing. **Feng Guo**: Conceptualization, Data curation, Funding acquisition, Project administration, Resources, Supervision, Writing - review & editing.

Declaration of competing interest

The authors declare that they have no known competing financial interests or personal relationships that could have appeared to influence the work reported in this paper.

Acknowledgments
The authors would like to acknowledge the support from the National Institutes of Health Awards (DP2AI160242, and U01DA056242) and the National Science Foundation Award (EFRI2422149). The authors also acknowledge the Indiana University Imaging Center (NIH1S10OD024988-01).

References
1. Lane CA, Hardy J, Schott JM. Alzheimer's disease. Eur J Neurol. 2018;25(1):59-70. Epub 2017/09/06. doi: 10.1111/ene.13439. PubMed PMID: 28872215.
2. DeTure MA, Dickson DW. The neuropathological diagnosis of Alzheimer's disease. Mol Neurodegener. 2019;14(1):32. Epub 2019/08/04. doi: 10.1186/s13024-019-0333-5. PubMed PMID: 31375134; PMCID: PMC6679484.
3. Scheltens P, De Strooper B, Kivipelto M, Holstege H, Chetelat G, Teunissen CE, Cummings J, van der Flier WM. Alzheimer's disease. Lancet. 2021;397(10284):1577-90. Epub 2021/03/06. doi: 10.1016/S0140-6736(20)32205-4. PubMed PMID: 33667416; PMCID: PMC8354300.
4. Dallemagne P, Rochais C. Facing the complexity of Alzheimer's disease. Future Med Chem. 2020;12(3):175-7. Epub 2019/11/22. doi: 10.4155/fmc-2019-0310. PubMed PMID: 31747794.
5. Bettcher BM, Tansey MG, Dorothee G, Heneka MT. Peripheral and central immune system crosstalk in Alzheimer disease - a research prospectus. Nat Rev Neurol. 2021;17(11):689-701. Epub 2021/09/16. doi: 10.1038/s41582-021-00549-x. PubMed PMID: 34522039; PMCID: PMC8439173 Association and a consultant to INmune Bio. G.D. is listed as an inventor on patent WO2014206899A1 related to a peripheral immunomodulatory approach for treating Alzheimer disease and related disorders, and on patent WO2018172540A1 related to peripheral immune biomarkers for predicting the progression of Alzheimer disease. The other authors declare no competing interests.
6. Jevtic S, Sengar AS, Salter MW, McLaurin J. The role of the immune system in Alzheimer disease: Etiology and treatment. Ageing Res Rev. 2017;40:84-94. Epub 2017/09/25. doi: 10.1016/j.arr.2017.08.005. PubMed PMID: 28941639.
7. Hansen DV, Hanson JE, Sheng M. Microglia in Alzheimer's disease. J Cell Biol. 2018;217(2):459-72. Epub 2017/12/03. doi: 10.1083/jcb.201709069. PubMed PMID: 29196460; PMCID: PMC5800817.
8. Heneka MT, Golenbock DT, Latz E. Innate immunity in Alzheimer's disease. Nat Immunol. 2015;16(3):229-36. Epub 2015/02/18. doi: 10.1038/ni.3102. PubMed PMID: 25689443.
9. Colonna M, Butovsky O. Microglia Function in the Central Nervous System During Health and Neurodegeneration. Annu Rev Immunol. 2017;35:441-68. Epub 2017/02/23. doi: 10.1146/annurev-immunol-051116-052358. PubMed PMID: 28226226; PMCID: PMC8167938.
10. Wu KM, Zhang YR, Huang YY, Dong Q, Tan L, Yu JT. The role of the immune system in Alzheimer's disease. Ageing Res Rev. 2021;70:101409. Epub 2021/07/18. doi: 10.1016/j.arr.2021.101409. PubMed PMID: 34273589.
11. Wennström M, Nielsen HM. Cell adhesion molecules in Alzheimer's disease. Degener Neurol Neuromuscul Dis. 2012;2:65-77. doi: 10.2147/DNND.S19829. PubMed PMID: 30890880.
12. Castellani G, Schwartz M. Immunological Features of Non-neuronal Brain Cells: Implications for Alzheimer's Disease Immunotherapy. Trends Immunol. 2020;41(9):794-804. Epub 2020/08/18. doi: 10.1016/j.it.2020.07.005. PubMed PMID: 32800704.
13. Munoz-Castro C, Mejias-Ortega M, Sanchez-Mejias E, Navarro V, Trujillo-Estrada L, Jimenez S, Garcia-Leon JA, Fernandez-Valenzuela JJ, Sanchez-Mico MV, Romero-Molina C, Moreno-Gonzalez I, Baglietto-Vargas D, Vizuete M, Gutierrez A, Vitorica J. Monocyte-derived cells invade brain parenchyma and amyloid plaques in human Alzheimer's disease hippocampus.

Acta Neuropathol Commun. 2023;11(1):31. Epub 2023/03/02. doi: 10.1186/s40478-023-01530-z. PubMed PMID: 36855152; PMCID: PMC9976401.
14. Cao W, Zheng H. Peripheral immune system in aging and Alzheimer's disease. Mol Neurodegener. 2018;13(1):51. Epub 2018/10/05. doi: 10.1186/s13024-018-0284-2. PubMed PMID: 30285785; PMCID: PMC6169078.
15. Zhou K, Han J, Wang Y, Xu Y, Zhang Y, Zhu C. The therapeutic potential of bone marrow-derived macrophages in neurological diseases. CNS Neurosci Ther. 2022;28(12):1942-52. Epub 2022/09/07. doi: 10.1111/cns.13964. PubMed PMID: 36066198; PMCID: PMC9627381.
16. Kiyota T, Gendelman HE, Weir RA, Higgins EE, Zhang G, Jain M. CCL2 affects beta-amyloidosis and progressive neurocognitive dysfunction in a mouse model of Alzheimer's disease. Neurobiol Aging. 2013;34(4):1060-8. Epub 2012/10/09. doi: 10.1016/j.neurobiolaging.2012.08.009. PubMed PMID: 23040664; PMCID: PMC4011558.
17. Garre JM, Yang G. Contributions of monocytes to nervous system disorders. J Mol Med (Berl). 2018;96(9):873-83. Epub 2018/07/22. doi: 10.1007/s00109-018-1672-3. PubMed PMID: 30030568; PMCID: PMC6186399.
18. Stamatovic SM, Shakui P, Keep RF, Moore BB, Kunkel SL, Van Rooijen N, Andjelkovic AV. Monocyte chemoattractant protein-1 regulation of blood-brain barrier permeability. J Cereb Blood Flow Metab. 2005;25(5):593-606. Epub 2005/02/04. doi: 10.1038/sj.jcbfm.9600055. PubMed PMID: 15689955.
19. Ao Z, Song S, Tian C, Cai H, Li X, Miao Y, Wu Z, Krzesniak J, Ning B, Gu M, Lee LP, Guo F. Understanding Immune-Driven Brain Aging by Human Brain Organoid Microphysiological Analysis Platform. Adv Sci (Weinh). 2022;9(27):e2200475. Epub 20220731. doi: 10.1002/advs.202200475. PubMed PMID: 35908805; PMCID: PMC9507385.
20. Theriault P, ElAli A, Rivest S. The dynamics of monocytes and microglia in Alzheimer's disease. Alzheimers Res Ther. 2015;7(1):41. Epub 2015/04/17. doi: 10.1186/s13195-015-0125-2. PubMed PMID: 25878730; PMCID: PMC4397873.
21. Feng Y, Li L, Sun XH. Monocytes and Alzheimer's disease. Neurosci Bull. 2011;27(2):115-22. Epub 2011/03/29. doi: 10.1007/s12264-011-1205-3. PubMed PMID: 21441973; PMCID: PMC5560348.
22. Malm T, Koistinaho M, Muona A, Magga J, Koistinaho J. The role and therapeutic potential of monocytic cells in Alzheimer's disease. Glia. 2010;58(8):889-900. Epub 2010/02/16. doi: 10.1002/glia.20973. PubMed PMID: 20155817.
23. Yan P, Kim KW, Xiao Q, Ma X, Czerniewski LR, Liu H, Rawnsley DR, Yan Y, Randolph GJ, Epelman S, Lee JM, Diwan A. Peripheral monocyte-derived cells counter amyloid plaque pathogenesis in a mouse model of Alzheimer's disease. J Clin Invest. 2022;132(11). Epub 2022/05/06. doi: 10.1172/JCI152565. PubMed PMID: 35511433; PMCID: PMC9151689.
24. Chen ZY, Zhang Y. Animal models of Alzheimer's disease: Applications, evaluation, and perspectives. Zool Res. 2022;43(6):1026-40. Epub 2022/11/02. doi: 10.24272/j.issn.2095-8137.2022.289. PubMed PMID: 36317468; PMCID: PMC9700500.
25. Dawson TM, Golde TE, Lagier-Tourenne C. Animal models of neurodegenerative diseases. Nat Neurosci. 2018;21(10):1370-9. Epub 2018/09/27. doi: 10.1038/s41593-018-0236-8. PubMed PMID: 30250265; PMCID: PMC6615039.
26. Drummond E, Wisniewski T. Alzheimer's disease: experimental models and reality. Acta Neuropathol. 2017;133(2):155-75. Epub 2016/12/28. doi: 10.1007/s00401-016-1662-x. PubMed PMID: 28025715; PMCID: PMC5253109.
27. Song HW, Foreman KL, Gastfriend BD, Kuo JS, Palecek SP, Shusta EV. Transcriptomic comparison of human and mouse brain microvessels. Sci Rep. 2020;10(1):12358. Epub 20200723. doi: 10.1038/s41598-020-69096-7. PubMed PMID: 32704093; PMCID: PMC7378255.
28. O'Brown NM, Pfau SJ, Gu C. Bridging barriers: a comparative look at the blood-brain barrier across organisms. Genes Dev. 2018;32(7-8):466-78. doi: 10.1101/gad.309823.117. PubMed PMID: 29692355; PMCID: PMC5959231.

29. Ormel PR, Vieira de Sa R, van Bodegraven EJ, Karst H, Harschnitz O, Sneeboer MAM, Johansen LE, van Dijk RE, Scheefhals N, Berdenis van Berlekom A, Ribes Martinez E, Kling S, MacGillavry HD, van den Berg LH, Kahn RS, Hol EM, de Witte LD, Pasterkamp RJ. Microglia innately develop within cerebral organoids. Nat Commun. 2018;9(1):4167. Epub 2018/10/12. doi: 10.1038/s41467-018-06684-2. PubMed PMID: 30301888; PMCID: PMC6177485 consultancy fees at Baxter International, and is a member of the scientific advisory board at Biogen Idec, Cytokinetics, and no other competing interests. All other authors declare no competing interests.
30. Ao Z, Cai H, Wu Z, Song S, Karahan H, Kim B, Lu HC, Kim J, Mackie K, Guo F. Tubular human brain organoids to model microglia-mediated neuroinflammation. Lab Chip. 2021;21(14):2751-62. doi: 10.1039/d1lc00030f. PubMed PMID: 34021557; PMCID: PMC8493632.
31. Qiao H, Zhao W, Guo M, Zhu L, Chen T, Wang J, Xu X, Zhang Z, Wu Y, Chen P. Cerebral Organoids for Modeling of HSV-1-Induced-Amyloid beta Associated Neuropathology and Phenotypic Rescue. Int J Mol Sci. 2022;23(11). Epub 2022/06/11. doi: 10.3390/ijms23115981. PubMed PMID: 35682661; PMCID: PMC9181143.
32. Grenier K, Kao J, Diamandis P. Three-dimensional modeling of human neurodegeneration: brain organoids coming of age. Mol Psychiatry. 2020;25(2):254-74. Epub 2019/08/25. doi: 10.1038/s41380-019-0500-7. PubMed PMID: 31444473.
33. Bi FC, Yang XH, Cheng XY, Deng WB, Guo XL, Yang H, Wang Y, Li J, Yao Y. Optimization of cerebral organoids: a more qualified model for Alzheimer's disease research. Transl Neurodegener. 2021;10(1):27. Epub 2021/08/11. doi: 10.1186/s40035-021-00252-3. PubMed PMID: 34372927; PMCID: PMC8349709.
34. Papaspyropoulos A, Tsolaki M, Foroglou N, Pantazaki AA. Modeling and Targeting Alzheimer's Disease With Organoids. Front Pharmacol. 2020;11:396. Epub 2020/04/18. doi: 10.3389/fphar.2020.00396. PubMed PMID: 32300301; PMCID: PMC7145390.
35. Bubnys A, Tsai LH. Harnessing cerebral organoids for Alzheimer's disease research. Curr Opin Neurobiol. 2022;72:120-30. Epub 2021/11/25. doi: 10.1016/j.conb.2021.10.003. PubMed PMID: 34818608.
36. Li K, Gu L, Cai H, Lu HC, Mackie K, Guo F. Human brain organoids for understanding substance use disorders. Drug Metab Pharmacokinet. 2024;58:101031. Epub 2024/08/16. doi: 10.1016/j.dmpk.2024.101031. PubMed PMID: 39146603.
37. Cai H, Ao Z, Hu L, Moon Y, Wu Z, Lu HC, Kim J, Guo F. Acoustofluidic assembly of 3D neurospheroids to model Alzheimer's disease. Analyst. 2020;145(19):6243-53. doi: 10.1039/d0an01373k. PubMed PMID: 32840509; PMCID: PMC7530134.
38. Ao Z, Wu Z, Cai H, Hu L, Li X, Kaurich C, Chang J, Gu M, Cheng L, Lu X, Guo F. Rapid Profiling of Tumor-Immune Interaction Using Acoustically Assembled Patient-Derived Cell Clusters. Adv Sci (Weinh). 2022;9(22):e2201478. Epub 20220525. doi: 10.1002/advs.202201478. PubMed PMID: 35611994; PMCID: PMC9353481.
39. Cai H, Ao Z, Wu Z, Song S, Mackie K, Guo F. Intelligent acoustofluidics enabled mini-bioreactors for human brain organoids. Lab Chip. 2021;21(11):2194-205. doi: 10.1039/d1lc00145k. PubMed PMID: 33955446; PMCID: PMC8243411.
40. Cai H, Ao Z, Tian C, Wu Z, Liu H, Tchieu J, Gu M, Mackie K, Guo F. Brain organoid reservoir computing for artificial intelligence. Nature Electronics. 2023;6(12):1032-9.
41. Gu L, Cai H, Chen L, Gu M, Tchieu J, Guo F. Functional Neural Networks in Human Brain Organoids. BME Front. 2024;5:0065. Epub 20240923. doi: 10.34133/bmef.0065. PubMed PMID: 39314749; PMCID: PMC11418062.
42. Wu Z, Cai H, Ao Z, Xu J, Heaps S, Guo F. Microfluidic Printing of Tunable Hollow Microfibers for Vascular Tissue Engineering. Adv Mater Technol. 2021;6(8). Epub 20210610. doi: 10.1002/admt.202000683. PubMed PMID: 34458563; PMCID: PMC8386518.
43. Ao Z, Cai H, Wu Z, Hu L, Nunez A, Zhou Z, Liu H, Bondesson M, Lu X, Lu X, Dao M, Guo F. Microfluidics guided by deep learning for cancer immunotherapy screening. Proc Natl Acad Sci

U S A. 2022;119(46):e2214569119. Epub 20221107. doi: 10.1073/pnas.2214569119. PubMed PMID: 36343225; PMCID: PMC9674214.
44. Ao Z, Cai H, Wu Z, Hu L, Li X, Kaurich C, Gu M, Cheng L, Lu X, Guo F. Evaluation of cancer immunotherapy using mini-tumor chips. Theranostics. 2022;12(8):3628-36. Epub 20220501. doi: 10.7150/thno.71761. PubMed PMID: 35664082; PMCID: PMC9131272.
45. Zhou Z, Van der Jeught K, Fang Y, Yu T, Li Y, Ao Z, Liu S, Zhang L, Yang Y, Eyvani H, Cox ML, Wang X, He X, Ji G, Schneider BP, Guo F, Wan J, Zhang X, Lu X. An organoid-based screen for epigenetic inhibitors that stimulate antigen presentation and potentiate T-cell-mediated cytotoxicity. Nat Biomed Eng. 2021;5(11):1320-35. Epub 20211101. doi: 10.1038/s41551-021-00805-x. PubMed PMID: 34725507; PMCID: PMC8647932.
46. Guo F, Li S, Caglar MU, Mao Z, Liu W, Woodman A, Arnold JJ, Wilke CO, Huang TJ, Cameron CE. Single-cell virology: on-chip investigation of viral infection dynamics. Cell reports. 2017;21(6):1692-704.
47. Cai H, Tian C, Chen L, Yang Y, Sun AX, McCracken K, Tchieu J, Gu M, Mackie K, Guo F. Vascular network-inspired diffusible scaffolds for engineering functional midbrain organoids. Cell Stem Cell. 2025. Epub 20250308. doi: 10.1016/j.stem.2025.02.010. PubMed PMID: 40101722.
48. Fiala M, Zhang L, Gan X, Sherry B, Taub D, Graves MC, Hama S, Way D, Weinand M, Witte MJMM. Amyloid-β induces chemokine secretion and monocyte migration across a human blood-brain barrier model1998;4:480-9.
49. Fani Maleki A, Rivest S. Innate Immune Cells: Monocytes, Monocyte-Derived Macrophages and Microglia as Therapeutic Targets for Alzheimer's Disease and Multiple Sclerosis. Front Cell Neurosci. 2019;13:355. Epub 2019/08/21. doi: 10.3389/fncel.2019.00355. PubMed PMID: 31427930; PMCID: PMC6690269.
50. Cai H, Ao Z, Tian C, Wu Z, Kaurich C, Chen Z, Gu M, Hohmann AG, Mackie K, Guo F. Engineering human spinal microphysiological systems to model opioid-induced tolerance. Bioact Mater. 2023;22:482-90. Epub 20221025. doi: 10.1016/j.bioactmat.2022.10.007. PubMed PMID: 36330161; PMCID: PMC9618681.
51. Ao Z, Cai H, Wu Z, Krzesniak J, Tian C, Lai YY, Mackie K, Guo F. Human Spinal Organoid-on-a-Chip to Model Nociceptive Circuitry for Pain Therapeutics Discovery. Anal Chem. 2022;94(2):1365-72. Epub 20211220. doi: 10.1021/acs.analchem.1c04641. PubMed PMID: 34928595.
52. Ao Z, Cai H, Havert DJ, Wu Z, Gong Z, Beggs JM, Mackie K, Guo F. One-Stop Microfluidic Assembly of Human Brain Organoids To Model Prenatal Cannabis Exposure. Anal Chem. 2020;92(6):4630-8. Epub 20200228. doi: 10.1021/acs.analchem.0c00205. PubMed PMID: 32070103.
53. Tian C, Cai H, Ao Z, Gu L, Li X, Niu VC, Bondesson M, Gu M, Mackie K, Guo F. Engineering human midbrain organoid microphysiological systems to model prenatal PFOS exposure. Sci Total Environ. 2024;947:174478. Epub 2024/07/05. doi: 10.1016/j.scitotenv.2024.174478. PubMed PMID: 38964381.
54. Garwood CJ, Cooper JD, Hanger DP, Noble W. Anti-inflammatory impact of minocycline in a mouse model of tauopathy. Front Psychiatry. 2010;1:136. Epub 2010/01/01. doi: 10.3389/fpsyt.2010.00136. PubMed PMID: 21423446; PMCID: PMC3059645.
55. Mora E, Guglielmotti A, Biondi G, Sassone-Corsi P. Bindarit: an anti-inflammatory small molecule that modulates the NFkappaB pathway. Cell Cycle. 2012;11(1):159-69. Epub 2011/12/23. doi: 10.4161/cc.11.1.18559. PubMed PMID: 22189654; PMCID: PMC3356824.
56. Arfaei R, Mikaeili N, Daj F, Boroumand A, Kheyri A, Yaraghi P, Shirzad Z, Keshavarz M, Hassanshahi G, Jafarzadeh A, Shahrokhi VM, Khorramdelazad H. Decoding the role of the CCL2/CCR2 axis in Alzheimer's disease and innovating therapeutic approaches: Keeping All options open. Int Immunopharmacol. 2024;135:112328. Epub 2024/05/27. doi: 10.1016/j.intimp.2024.112328. PubMed PMID: 38796962.

57. Motaghinejad M, Motevalian M. Neuroprotective Properties of Minocycline Against Methylphenidate-Induced Neurodegeneration: Possible Role of CREB/BDNF and Akt/GSK3 Signaling Pathways in Rat Hippocampus. Neurotox Res. 2022;40(3):689-713. Epub 20220421. doi: 10.1007/s12640-021-00454-7. PubMed PMID: 35446003.
58. Heneka MT, Carson MJ, Khoury JE, Landreth GE, Brosseron F, Feinstein DL, Jacobs AH, Wyss-Coray T, Vitorica J, Ransohoff RM, Herrup K, Frautschy SA, Finsen B, Brown GC, Verkhratsky A, Yamanaka K, Koistinaho J, Latz E, Halle A, Petzold GC, Town T, Morgan D, Shinohara ML, Perry VH, Holmes C, Bazan NG, Brooks DJ, Hunot S, Joseph B, Deigendesch N, Garaschuk O, Boddeke E, Dinarello CA, Breitner JC, Cole GM, Golenbock DT, Kummer MP. Neuroinflammation in Alzheimer's disease. The Lancet Neurology. 2015;14(4):388-405. doi: 10.1016/s1474-4422(15)70016-5.
59. Calsolaro V, Edison P. Neuroinflammation in Alzheimer's disease: Current evidence and future directions. Alzheimers Dement. 2016;12(6):719-32. Epub 2016/05/18. doi: 10.1016/j.jalz.2016.02.010. PubMed PMID: 27179961.
60. Phillips EC, Croft CL, Kurbatskaya K, O'Neill MJ, Hutton ML, Hanger DP, Garwood CJ, Noble W. Astrocytes and neuroinflammation in Alzheimer's disease. Biochem Soc Trans. 2014;42(5):1321-5. Epub 2014/09/19. doi: 10.1042/BST20140155. PubMed PMID: 25233410.
61. Michaud JP, Bellavance MA, Prefontaine P, Rivest S. Real-time in vivo imaging reveals the ability of monocytes to clear vascular amyloid beta. Cell Rep. 2013;5(3):646-53. Epub 2013/11/12. doi: 10.1016/j.celrep.2013.10.010. PubMed PMID: 24210819.
62. Conductier G, Blondeau N, Guyon A, Nahon JL, Rovere C. The role of monocyte chemoattractant protein MCP1/CCL2 in neuroinflammatory diseases. J Neuroimmunol. 2010;224(1-2):93-100. Epub 2010/08/04. doi: 10.1016/j.jneuroim.2010.05.010. PubMed PMID: 20681057.
63. Mildner A, Schlevogt B, Kierdorf K, Bottcher C, Erny D, Kummer MP, Quinn M, Bruck W, Bechmann I, Heneka MT, Priller J, Prinz M. Distinct and non-redundant roles of microglia and myeloid subsets in mouse models of Alzheimer's disease. J Neurosci. 2011;31(31):11159-71. Epub 2011/08/05. doi: 10.1523/JNEUROSCI.6209-10.2011. PubMed PMID: 21813677; PMCID: PMC6623351.
64. Guedes JR, Lao T, Cardoso AL, El Khoury J. Roles of Microglial and Monocyte Chemokines and Their Receptors in Regulating Alzheimer's Disease-Associated Amyloid-beta and Tau Pathologies. Front Neurol. 2018;9:549. Epub 2018/08/31. doi: 10.3389/fneur.2018.00549. PubMed PMID: 30158892; PMCID: PMC6104478.
65. Li S, Hayden EY, Garcia VJ, Fuchs DT, Sheyn J, Daley DA, Rentsendorj A, Torbati T, Black KL, Rutishauser U, Teplow DB, Koronyo Y, Koronyo-Hamaoui M. Activated Bone Marrow-Derived Macrophages Eradicate Alzheimer's-Related Abeta(42) Oligomers and Protect Synapses. Front Immunol. 2020;11:49. Epub 2020/02/23. doi: 10.3389/fimmu.2020.00049. PubMed PMID: 32082319; PMCID: PMC7005081.
66. Koronyo Y, Salumbides BC, Sheyn J, Pelissier L, Li S, Ljubimov V, Moyseyev M, Daley D, Fuchs DT, Pham M, Black KL, Rentsendorj A, Koronyo-Hamaoui M. Therapeutic effects of glatiramer acetate and grafted CD115(+) monocytes in a mouse model of Alzheimer's disease. Brain. 2015;138(Pt 8):2399-422. Epub 2015/06/07. doi: 10.1093/brain/awv150. PubMed PMID: 26049087; PMCID: PMC4840949.
67. Martin E, Boucher C, Fontaine B, Delarasse C. Distinct inflammatory phenotypes of microglia and monocyte-derived macrophages in Alzheimer's disease models: effects of aging and amyloid pathology. Aging Cell. 2017;16(1):27-38. Epub 2016/10/11. doi: 10.1111/acel.12522. PubMed PMID: 27723233; PMCID: PMC5242297.
68. Tian C, Ao Z, Cerneckis J, Cai H, Chen L, Niu H, Takayama K, Kim J, Shi Y, Gu M, Kanekiyo T, Guo F. Understanding monocyte-driven neuroinflammation in Alzheimer's disease using human brain organoid microphysiological systems. bioRxiv. 2025. Epub 20250220. doi: 10.1101/2025.02.16.638539. PubMed PMID: 40027735; PMCID: PMC11870548.

69. Garofalo S, Cocozza G, Bernardini G, Savage J, Raspa M, Aronica E, Tremblay ME, Ransohoff RM, Santoni A, Limatola C. Blocking immune cell infiltration of the central nervous system to tame Neuroinflammation in Amyotrophic lateral sclerosis. Brain Behav Immun. 2022;105:1-14. Epub 20220607. doi: 10.1016/j.bbi.2022.06.004. PubMed PMID: 35688338.
70. Romero-Miguel D, Lamanna-Rama N, Casquero-Veiga M, Gomez-Rangel V, Desco M, Soto-Montenegro ML. Minocycline in neurodegenerative and psychiatric diseases: An update. Eur J Neurol. 2021;28(3):1056-81. Epub 2020/11/13. doi: 10.1111/ene.14642. PubMed PMID: 33180965.
71. Niu F, Liao K, Hu G, Sil S, Callen S, Guo ML, Yang L, Buch S. Cocaine-induced release of CXCL10 from pericytes regulates monocyte transmigration into the CNS. J Cell Biol. 2019;218(2):700-21. Epub 20190109. doi: 10.1083/jcb.201712011. PubMed PMID: 30626719; PMCID: PMC6363463.
72. Chen S, Guo D, Zhu Y, Xiao S, Xie J, Zhang Z, Hu Y, Huang J, Ma X, Ning Z, Cao L, Cheng J, Tang Y. Amyloid beta oligomer induces cerebral vasculopathy via pericyte-mediated endothelial dysfunction. Alzheimers Res Ther. 2024;16(1):56. Epub 20240312. doi: 10.1186/s13195-024-01423-w. PubMed PMID: 38475929; PMCID: PMC10935813.
73. Floryanzia SD, Nance E. Applications and Considerations for Microfluidic Systems To Model the Blood-Brain Barrier. ACS Appl Bio Mater. 2023;6(9):3617-32. Epub 20230815. doi: 10.1021/acsabm.3c00364. PubMed PMID: 37582179; PMCID: PMC11646049.
74. Zhao Y, Demirci U, Chen Y, Chen P. Multiscale brain research on a microfluidic chip. Lab Chip. 2020;20(9):1531-43. Epub 20200309. doi: 10.1039/c9lc01010f. PubMed PMID: 32150176.
75. Sweeney MD, Sagare AP, Zlokovic BV. Blood-brain barrier breakdown in Alzheimer disease and other neurodegenerative disorders. Nat Rev Neurol. 2018;14(3):133-50. Epub 2018/01/30. doi: 10.1038/nrneurol.2017.188. PubMed PMID: 29377008; PMCID: PMC5829048.
76. Peng B, Hao S, Tong Z, Bai H, Pan S, Lim KL, Li L, Voelcker NH, Huang W. Blood-brain barrier (BBB)-on-a-chip: a promising breakthrough in brain disease research. Lab Chip. 2022;22(19):3579-602. Epub 2022/08/26. doi: 10.1039/d2lc00305h. PubMed PMID: 36004771.

Figure and captions

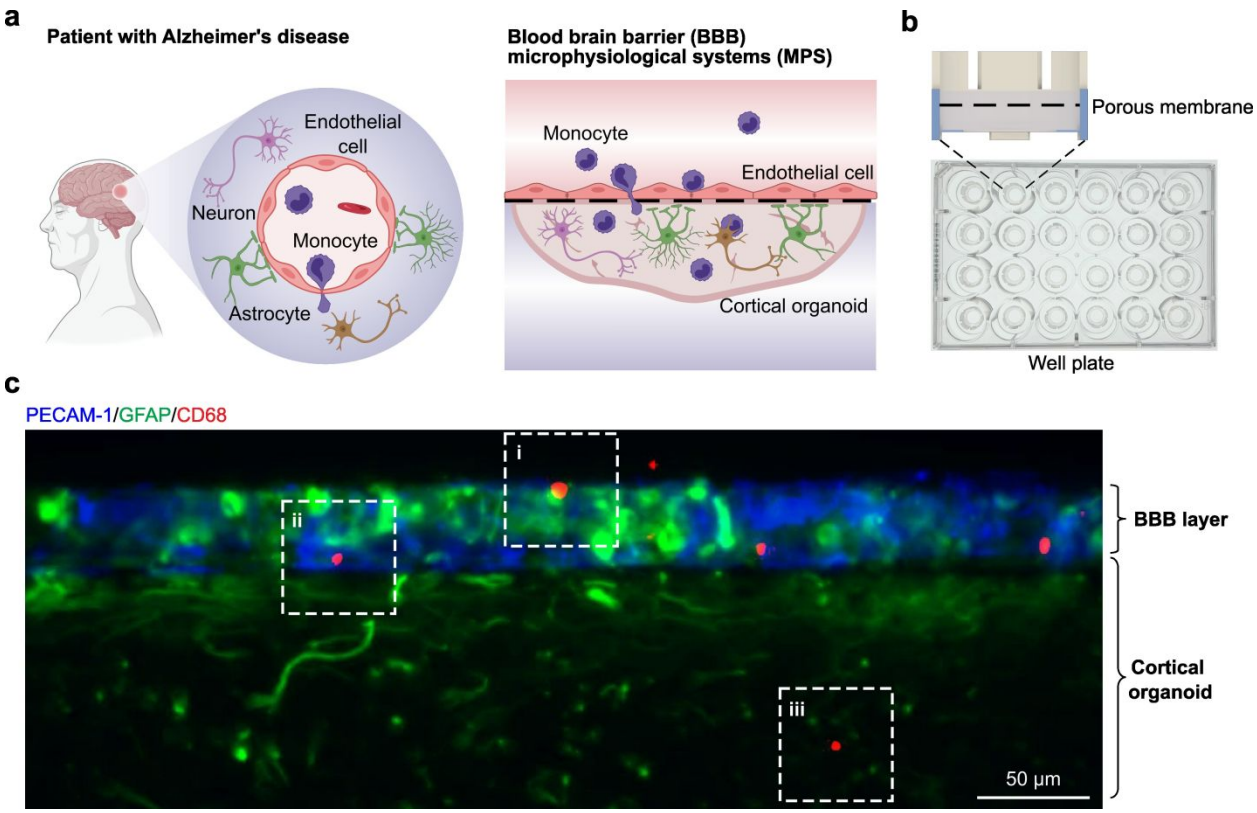

Figure 1. Engineering BBB-MPS models for recapitulating dynamic penetration and infiltration of AD monocytes. a, Schematics showing the penetration and infiltration of monocytes and the subsequent neuroimmune interactions in AD patients (left) and the BBB-MPS model for recapitulating the same process. **b,** A 24-well plate with 24 BBB-MPS models. **c,** Immunofluorescent image of the BBB-MPS models after 48 h treatment with AD patient-derived monocytes.

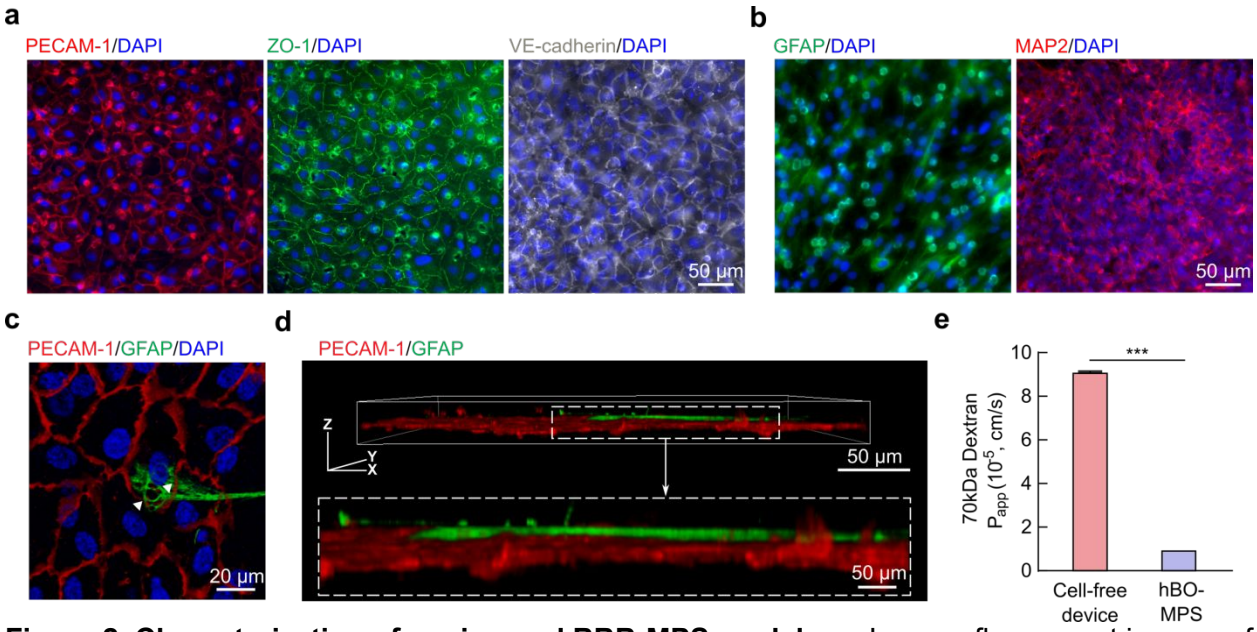

Figure 2. Characterization of engineered BBB-MPS models. a, Immunofluorescent images of the BBB labeled with PECAM-1, ZO-1, and VE-cadherin. **b,** Immunofluorescent images of the cortical organoids labeled with GFAP and MAP2. Top view (**c**) and side view (**d**) showing GFAP-labeled astrocytes extending end-feet to wrap around PECAM-1 labeled endothelium. **e,** The permeability of dextran (70 kDa) was compared in cell-free devices and BBB-MPSs. Data are presented as mean ± SEM

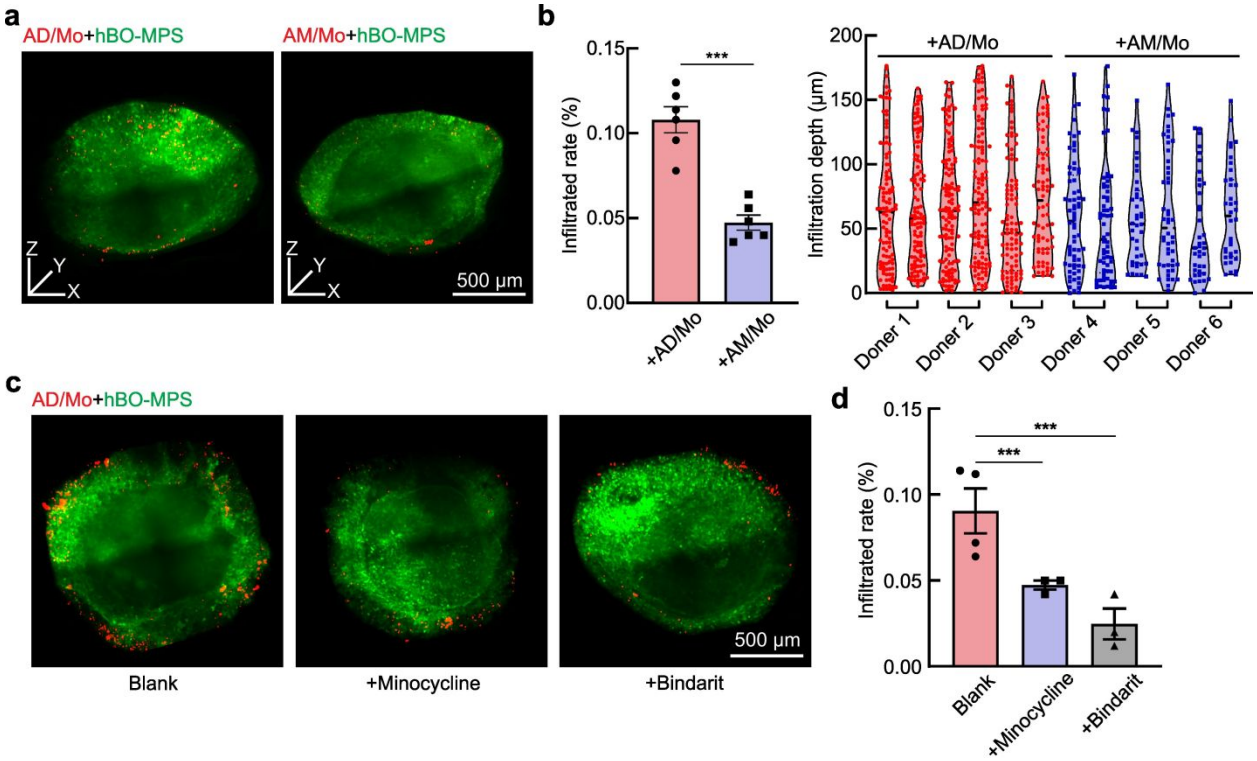

Figure 3. Characterization and intervention of AD monocyte infiltration of BBB-MPS models. a, Comparison of infiltration capacity of monocytes isolated from AD patients (>70-year-old, as AD/Mo) with monocytes isolated from age-matched control individuals (as AM/Mo). Scale bar: 500 μm. **b,** Quantification of infiltrated rate (left) and infiltration depth (right) between AD/Mo and AM/Mo. **c,** Comparison of infiltration capacity of AD monocytes after the Minocycline (Minocycline+) and Bindarit (Bindarit+) treatments. Scale bar: 500 μm. **d,** Quantification of infiltrated rate. Data are presented as mean ± SEM

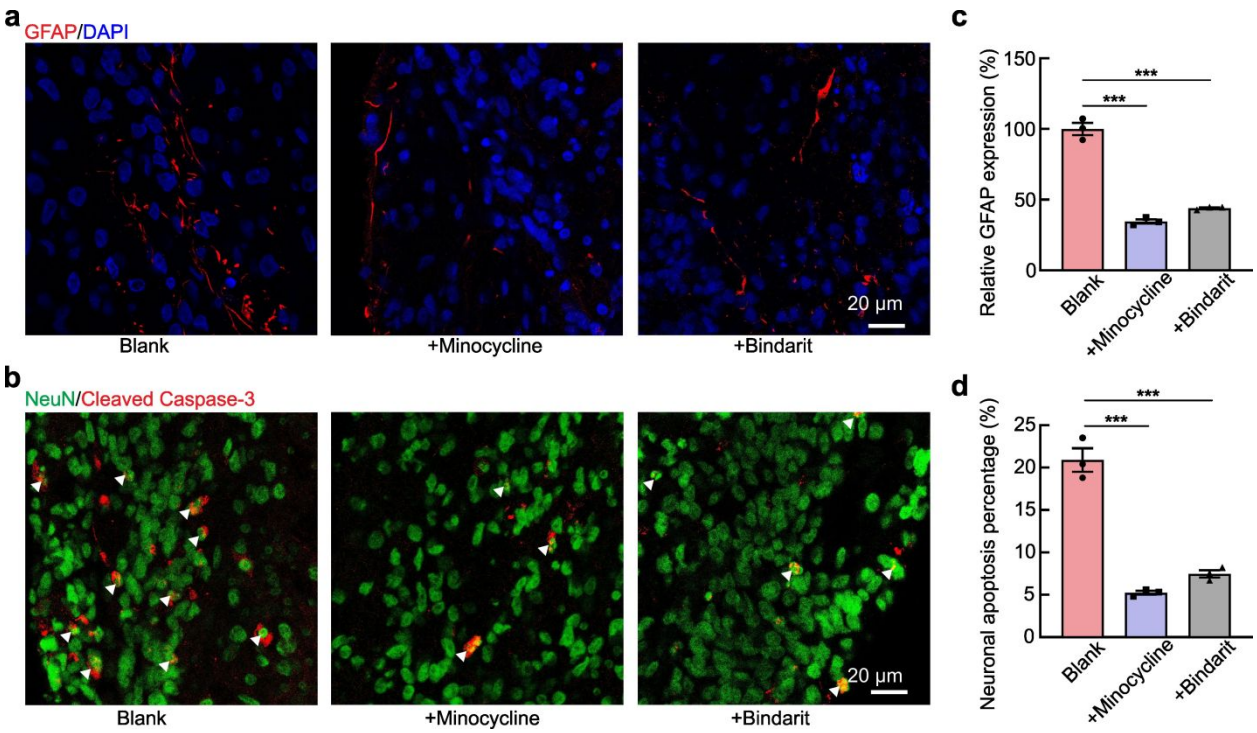

Figure 4. Investigation and intervention of AD monocyte-mediated neuroinflammation and neuronal apoptosis. a, The expression of GFAP was identified by immunofluorescence staining and the quantifications. **b,** The expression of NeuN and cleaved Caspase 3 was identified by immunofluorescence staining, and the quantifications for **c,** relative GFAP fluorescence intensity statistics, and **d,** neuronal apoptosis percentage. Scale bars: 20 μm. Data are presented as mean ± SEM

Data Availability Statement

The data supporting this article have been included as part of the Supplementary Information.